Received: 28 July 2020 | Revised: 4 March 2021 | Accepted: 15 March 2021

DOI: 10.1111/btp.12964

bioTROPICA ASSOCIATION FOR TROPICAL BIOLOGY AND CONSERVATION WILEY

ORIGINAL ARTICLE

Hydraulic architecture explains species moisture dependency but not mortality rates across a tropical rainfall gradient

Alexandria L. Pivovaroff[1] | Brett T. Wolfe[2,3] | Nate McDowell[1] | Bradley Christoffersen[4] | Stuart Davies[2] | L. Turin Dickman[5] | Charlotte Grossiord[6,7] | Riley T. Leff[1] | Alistair Rogers[8] | Shawn P. Serbin[8] | S. Joseph Wright[2] | Jin Wu[8,9] | Chonggang Xu[5] | Jeffrey Q. Chambers[10]

[1]Atmospheric Science and Global Change Division, Pacific Northwest National Laboratory, Richland, WA, USA

[2]Smithsonian Tropical Research Institute, Balboa, Republic of Panama

[3]School of Renewable Natural Resources, Louisiana State University, Baton Rouge, LA, USA

[4]Department of Biology, University of Texas Rio Grande Valley, Brownsville, TX, USA

[5]Earth and Environmental Sciences Division, Los Alamos National Laboratory, Los Alamos, NM, USA

[6]Functional Plant Ecology, Community Ecology Unit, Swiss Federal Institute for Forest, Snow and Landscape Research (WSL), Lausanne, Switzerland

[7]School of Architecture, Civil and Environmental Engineering ENAC, Plant Ecology Research Laboratory – PERL, EPFL, Lausanne, Switzerland

[8]Brookhaven National Laboratory, Environmental and Climate Sciences, Upton, NY, USA

[9]School of Biological Sciences, The University of Hong Kong, Hong Kong, Hong Kong

[10]Lawrence Berkeley National Laboratory, Earth and Environmental Science Area, Berkeley, CA, USA

Correspondence
Alexandria L. Pivovaroff, Atmospheric Science and Global Change Division, Pacific Northwest National Laboratory, Richland, WA 99354, USA.
Email: alexandria.pivovaroff@pnnl.gov

Funding information
Department of Energy, Grant/Award Number: DE-SC0012704; Office of Biological and Environmental Research in the Department of Energy, Office of Science; National Science Foundation, Grant/Award Number: DEB-00753102, DEB-0129874, DEB-0346488, DEB-0425651, DEB-0640386, DEB-9615226 and DEB-9909347

Associate Editor: Ferry Slik
Handling Editor: Heidi Asbjørnsen

Abstract

Intensified droughts are affecting tropical forests across the globe. However, the underlying mechanisms of tree drought response and mortality are poorly understood. Hydraulic traits and especially hydraulic safety margins (HSMs), that is, the extent to which plants buffer themselves from thresholds of water stress, provide insights into species-specific drought vulnerability. We investigated hydraulic traits during an intense drought triggered by the 2015–2016 El Niño on 27 canopy tree species across three tropical forest sites with differing precipitation. We capitalized on the drought event as a time when plant water status might approach or exceed thresholds of water stress. We investigated the degree to which these traits varied across the rainfall gradient, as well as relationships among hydraulic traits and species-specific optimal moisture and mortality rates. There were no differences among sites for any measured trait. There was strong coordination among traits, with a network analysis revealing two major groups of coordinated traits. In one group, there were water potentials, turgor loss point, sapwood capacitance and density, HSMs, and mortality rate. In the second group, there was leaf mass per area, leaf dry matter content, hydraulic architecture (leaf area to sapwood area ratio), and species-specific optimal moisture. These results demonstrated that while species with greater safety from turgor loss had lower mortality rates, hydraulic architecture was the only trait that

explained species' moisture dependency. Species with a greater leaf area to sapwood area ratio were associated with drier sites and reduced their transpirational demand during the dry season via deciduousness.

Abstract in Spanish is available with online material.

KEYWORDS
drought, El Niño, hydraulic safety margins, leaf mass per area, sapwood capacitance, tropical forest, turgor loss point, water potential

1 | INTRODUCTION

Climate change, including intensified and more frequent drought (Trenberth et al., 2014), is driving tree mortality and leading to forest degradation across the globe (Allen et al., 2015) and in many tropical forests (McDowell, 2018). Mortality rates vary widely among species (Brienen et al., 2015; Condit et al., 1995, 2017), suggesting a diversity of underlying physiological drought adaptation traits that can vary both within and across sites (Anderegg, 2015). However, we do not yet have a complete picture of the processes and mechanisms underlying tree drought response and mortality. Understanding the mechanisms of tropical forest responses to drought has implications for tropical forest functioning and can help answer unresolved questions concerning the mechanisms of tree mortality (Hartmann et al., 2015).

Hydraulic traits and water relations play a crucial role in plant drought responses and act as key determinants of safety from hydraulic failure (Blackman et al., 2016; Brodribb & Cochard, 2009). They regulate plant water use and influence a number of physiological processes. Hence, hydraulic traits can provide insights into how plants respond to abiotic stress (Anderegg et al., 2016; Meinzer & McCulloh, 2013), including acute drought. Drought can limit soil moisture availability for plant transpiration and thus cause reductions in plant water status, that is, water potential. As plants lose water, increased tension in the water column and declining water potential are coordinated with stomatal closure to slow desiccation (Martin-StPaul et al., 2017). However, plant dehydration does not completely stop with stomatal closure as water can still be lost via cuticular conductance (Kerstiens, 1996, 2006). Continued water loss can lead to the depletion of stored water as well as the introduction of embolism in xylem conduits via cavitation. Embolized, or air-filled, xylem conduits cannot transport water; hence, hydraulic conductance declines, and as more emboli occur, plants can become subject to hydraulic failure (Sperry & Love, 2015). Some species have a suite of coordinated traits that support greater drought tolerance, while other species are highly susceptible to drought (Pivovaroff et al., 2016). For example, more negative turgor loss point, greater sapwood density, sapwood capacitance, and resistance to xylem cavitation can all contribute to drought adaptation.

One key metric of drought mortality risk is the hydraulic safety margin (Anderegg et al., 2016; Nardini et al., 2013). Hydraulic safety margins (HSMs) are the difference between thresholds of water stress and the minimum water status that a plant experiences (Ψ_{MIN}). Different thresholds of water stress include xylem vulnerability to cavitation (i.e., the water potential at 50% or 88% percent loss of hydraulic conductivity; Ψ_{50} and $\Psi_{88,}$ respectively), leaf wilting (i.e., the water potential at the turgor loss point; π_{TLP}), and the water potential at which sapwood capacitance is diminished (i.e., the water potential at the "elbow" of the cumulative water release curve, here called C_{ELBOW}, described in Meinzer et al., 2009). The closer the water status of a plant comes to reaching its hydraulic threshold for water stress, the more likely the plant is to suffer hydraulic dysfunction. HSMs are potentially important traits in predicting tree death (Anderegg et al., 2016, but see Wolfe, 2017). While one might expect HSMs to be narrower at sites with lower mean annual precipitation, Choat et al. (2012) concluded that a majority of forest species operate within narrow HSMs (Ψ_{MIN}–Ψ_{50}), suggesting a convergence in vulnerability to drought across the planet regardless of mean annual precipitation (Choat et al., 2012). However, only 14 of the observed HSMs in that study were for tropical forest trees. Additionally, within a given site, HSMs can vary widely among species (Pivovaroff et al., 2018). Our understanding of mortality risk and HSMs for tropical species is limited, and to our knowledge, this has not been investigated for a wide selection of tropical tree species across sites with different long-term precipitation nor during an acute drought event.

Environmental conditions play a major role in the distribution and abundance of tropical tree species. For example, soil nutrient limitation and precipitation have long been recognized as key factors in shaping tropical forest plant communities (Baillie et al., 1987; Bongers et al., 1999; Gentry, 1988). In fact, multiple studies have found species-specific drought sensitivity in particular governs species distribution across the rainfall gradient that spans the isthmus of Panama (Condit et al., 2013; Engelbrecht et al., 2007). For example, Engelbrecht et al. (2007) analyzed 48 tropical tree and shrub species across 122 sites and found that soil water availability was a direct determinant of species distribution across local and regional scales. In addition, Condit et al. (2013) examined the responses of 550 tropical tree species across 72 sites in Panama to eight environmental factors, including dry-season intensity and soil fertility, and found that dry-season intensity and soil phosphorus were the strongest predictors of species occurrence. Using fitted coefficients from Condit et al. (2013) that relate species' probability of occurrence to dry-season intensity, one can calculate individual species optimal position across this same precipitation gradient, or species-specific

optimal moisture. Higher optimal moisture values mean a species is more highly associated with wet sites and therefore is more moisture-dependent. Understanding the correlations among species' moisture requirements, mortality rates, and hydraulic traits is critical to predict tropical forest responses to climate change.

The goal of this research was to examine how plant hydraulic traits vary among a diverse set of dominant tree species across a tropical rainfall gradient and to relate these traits to species-specific optimal moisture and mortality rates. To this end, we measured water potentials to determine the minimum seasonal water potential and the difference between the minimum seasonal water potential and the maximum seasonal water potential; pressure–volume curves to determine turgor loss point; water release curves to determine sapwood capacitance, the water potential at the "elbow" of the water release curve, and sapwood density; and morphological leaf traits including leaf mass per area, leaf dry matter content, and leaf area to sapwood area ratio. From these traits, we also calculated two HSMs: Ψ_{MIN}–π_{TLP} and Ψ_{MIN}–C_{ELBOW}. We conducted this research during an intense drought triggered by the 2015–2016 El Niño, capitalizing on this event as a time when plant water status might approach or exceed thresholds of water stress (i.e., small or possibly negative HSMs). We hypothesized that (1) hydraulic traits would vary across sites with different long-term mean annual precipitation following coordinated drought strategies, (2) species' hydraulic traits would be coordinated with their moisture dependency (i.e., less moisture-dependent species would be more drought-tolerant and have multiple metrics of drought safety as indicated by their suite of traits) and mortality rate, and (3) HSMs specifically would be highly coordinated with others traits in a hydraulic trait network.

2 | METHODS

2.1 | Study sites and species

This study was conducted at three lowland tropical forest sites on the isthmus of Panama with varying precipitation (Figure 1a and b). This region has a distinct wet season and dry season, with the majority of rainfall (>75%) occurring during the wet season (May–November). The first site, Parque Natural Metropolitano (PNM; 8°58′N, 79°34′W), is a seasonally dry forest with a mean annual precipitation of 1850 mm. The second site, Barro Colorado Island (BCI, 9°10′N, 79°51′W), is a lowland tropical moist forest with a mean annual precipitation of 2623 mm. The third site, Fort San Lorenzo (SLZ, 9°17′N, 79°58′W), is a wet evergreen forest with a mean annual precipitation of 3,300 mm (Figure 1). Monthly precipitation summaries for each site were downloaded from the Smithsonian Tropical Research Institute "Physical Monitoring Program" site (http://bioge odb.stri.si.edu/physical_monitoring/research/).

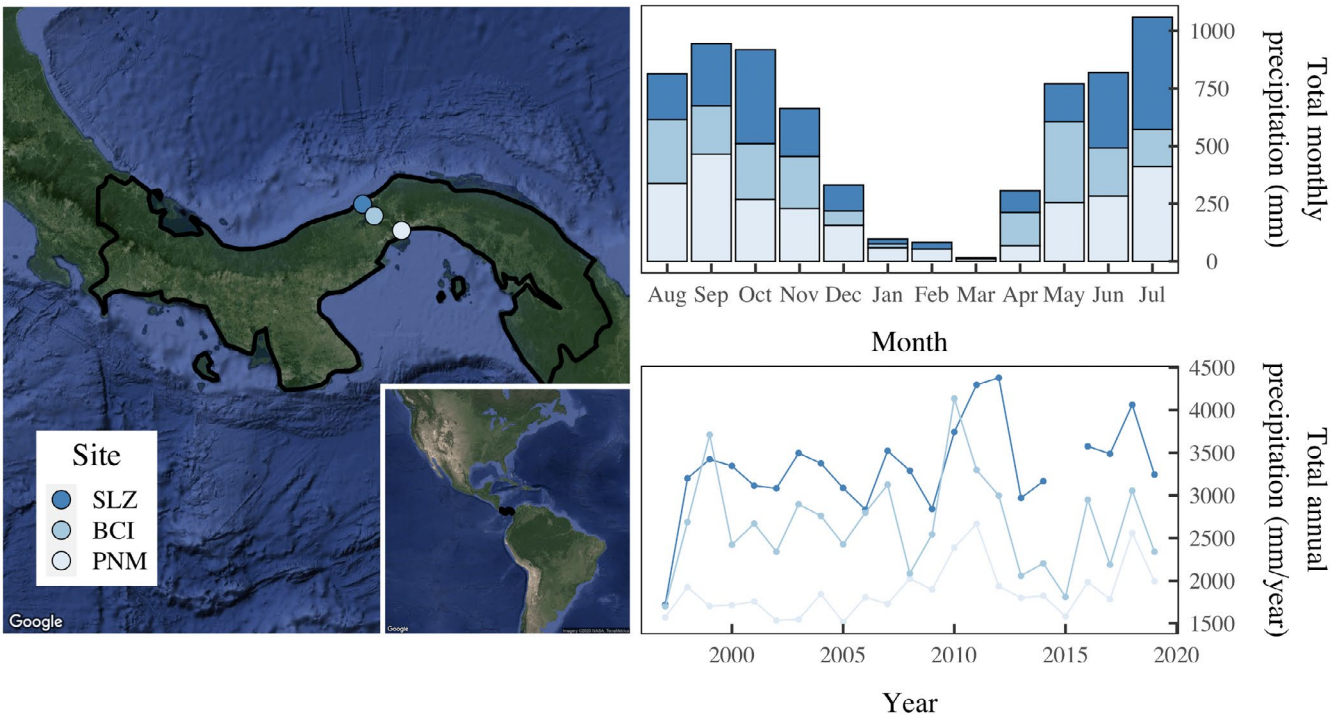

FIGURE 1 Map of North and South America with the location of Panama outlined in black (white inset box), with a close-up of the Republic of Panama and the three study sites, Parque Natural Metropolitano (PNM; light blue), Barro Colorado Island (BCI; medium blue), and Fort San Lorenzo (SLZ; dark blue). These sites capture a precipitation gradient across the Isthmus of Panama, as presented by the differences in total monthly precipitation (mm) as well as long-term differences in total annual precipitation (mm/year) from 1997 to 2019. Seasonal patterns reveal the majority of rainfall occurs during the wet season (May–November), and long-term patterns demonstrate that of the three study sites, SLZ has the highest precipitation and PNM has the lowest precipitation

Nine locally abundant canopy tree species (PNM n = 9, BCI n = 9, SLZ n = 9) were selected at each site, for a total of 27 tree species (Table 1). Species were selected with the criteria of (1) occurring within the footprint of the canopy crane for sample access (except at BCI, which has no canopy crane), (2) having leaves at the time of measurement, and (3) spanning a range of wood densities within each site (Table 1). Traits were measured on fully expanded, upper canopy sunlit leaves for one individual of each target species, except for pressure–volume curves and water release curves, for which multiple individuals of each species were used. The PNM and SLZ sites have canopy access cranes that allowed sampling at the top of the forest canopy. However, BCI did not have a canopy access crane, and instead leaves were sampled from two telecommunication towers or by slingshot. Field campaigns to measure seasonal water potential occurred each month (February–May) of the dry season during the 2015–2016 El Niño event that was associated with anomalously low annual precipitation at each site, except at BCI where water potential measurements were limited to a single field campaign.

2.2 | Leaf water potentials

Leaf water potential (Ψ; MPa) was measured on at least three leaves per tree for each study species during each field campaign using a Scholander-type pressure chamber to determine plant water status (PMS Instrument Co., Albany, OR, USA) over the course of the day, including predawn and midday. We defined the most negative water potential each species experienced over the course of the dry season as the minimum seasonal water potential (Ψ_{MIN}) (Bhaskar & Ackerly, 2006). In addition, $\Delta\Psi$ was defined as the difference between Ψ_{MIN} and the maximum water potential during our measurement period.

2.3 | Leaf and stem traits

Following leaf water potential measurement, leaves were processed for additional traits. Leaf dry matter content (LDMC; g/g) and leaf mass per area (LMA; g/m^2) were measured by collecting a known leaf area using a cork borer, weighing it with a precision balance for fresh mass

TABLE 1 27 canopy tree species from Parque Natural Metropolitano (n = 9), Barro Colorado Island (n = 9), and Fort San Lorenzo (n = 9) used for this study, with mean sapwood density and standard deviation, and leaf phenology

Site	Species	Sapwood density ± *SD* (g/cm^3)	Deciduous/Evergreen
Parque Natural Metropolitano	*Albizia adinocephala*	0.62 ± 0.08	Deciduous
	Anacardium excelsum	0.41 ± 0.054	Brevideciduous
	Pittoniotis trichantha	0.46 ± 0.041	Facultative deciduous
	Calycophyllum candidissimum	0.60 ± 0.04	Evergreen
	Castilla elastica	0.42 ± 0.034	Facultative deciduous
	Cordia alliodora	0.36 ± 0.02	Facultative deciduous
	Ficus insipida	0.45 ± 0.061	Brevideciduous
	Luehea seemannii	0.33 ± 0.045	Facultative deciduous
	Pseudobombax septenatum	0.39 ± 0.074	Obligate deciduous
Barro Colorado Island	*Alseis blackiana*	0.47 ± 0.013	Facultative deciduous
	Gustavia superba	0.47 ± 0.041	Evergreen
	Hura crepitans	0.45 ± 0.028	Facultative deciduous
	Inga pezizifera	0.59 ± 0.019	Evergreen
	Miconia argentea	0.56 ± 0.037	Evergreen
	Schizolobium parahyba	0.42 ± 0.102	Deciduous
	Simarouba amara	0.46 ± 0.01	Evergreen
	Spondias radlkoferi	0.41 ± 0.022	Facultative deciduous
	Tabebuia rosea	o.46 ± 0.014	Facultative deciduous
Fort San Lorenzo	*Apeiba membranaceae*	0.35 ± 0.034	Facultative deciduous
	Carapa guianensis	0.46 ± 0.028	Facultative deciduous
	Guatteria dumetorum	0.48 ± 0.059	Evergreen
	Miconia minutiflora	0.56 ± 0.022	Evergreen
	Tachigali versicolor	0.71 ± 0.019	Evergreen
	Terminalia amazonia	0.68 ± 0.027	Brevideciduous
	Tocoyena pittieri	0.69 ± 0.016	Evergreen
	Virola multiflora	0.50 ± 0.026	Evergreen
	Vochysia ferruginea	0.53 ± 0.017	Evergreen

(Fisher Science Education, Model SNL303, Hanover Park, IL), then hydrating it for saturated mass, and finally drying it in an oven at 70°C for at least 48 hr until reaching a constant mass to determine dry mass. LDMC was determined as leaf dry mass (g) divided by saturated mass (g). LMA was determined as leaf dry mass (g) divided by fresh area (m^2).

From three to five terminal branches on each individual, cross-sectional sapwood area, leaf area to sapwood area (A_L:A_{SW}), and sapwood density (ρ_{SW}) were measured. Sapwood area (cm^2) was determined by removing bark from a 1-cm length of each sample and using digital calipers to measure sapwood diameter and pith diameter, and calculating the sapwood area minus the pith area. The total distal leaf area for each sample was measured with a leaf area meter (LI-3100C, LI-COR, Lincoln, NE, USA), to calculate A_L:A_{SW} (m^2/m^2). ρ_{SW} was measured on fresh sapwood samples about 1 cm in diameter, with the bark and pith removed. We used the water displacement method (Osazuwa-Peters et al., 2011; Williamson & Wiemann, 2010) by attaching the sample to a needle and submerging the sample in a reservoir of water on a digital balance to determine the volume of water displaced by the sample, and then drying the samples in a drying oven at 70°C for at least 72 hr until reaching a constant mass to determine dry mass. ρ_{SW} was calculated as the ratio of dry mass (g) to fresh volume (cm^{-3}).

2.4 | Pressure–volume curves

From the same target trees and others nearby, additional mature shoots with recently mature leaves were collected to measure hydraulics traits including pressure–volume curves and vulnerability curves (see below). Two to six pressure–volume curves per species were measured following Koide et al. (1991), with the modification of determining leaf water potential on leaf disks with a psychrometer (J.R.D. Merrill Specialty Equipment, Logan, Utah, USA). This method has been shown to give results similar to those of the pressure chamber method (Nardini et al., 2008). For each curve, a single leaf disk was progressively dried on the bench, with weight and water potential measured at intervals to construct the pressure–volume curves. Subsequently, samples were placed in a drying oven at 70°C for at least 48 hr until reaching a constant mass to determine dry mass. The typical time to complete a measurement for each leaf disk was 4–5 hr, with full curves taking multiple days. From the pressure–volume curves, we calculated the water potential at turgor loss (π_{TLP}; MPa). Raw pressure–volume curves with fitted functions are provided in Figure S1, and box plots of TLP values for each curve by species are provided in Figure S2.

2.5 | Sapwood capacitance

Sapwood capacitance was measured via water release curves (Meinzer et al., 2003; Tyree & Ewers, 1991). For each species, three branches were collected from the crowns of 2–3 trees. Upon collection, the branches were sealed in opaque plastic bags and transported to the laboratory. Stem sections located 80–100 cm from the apex were used for measurements. A sapwood sample (i.e., secondary xylem, pith removed) 4 cm in length was removed from each stem. While removing the samples, the stem sections were enveloped in moist paper towels to ensure that samples did not dry. The samples were weighed for fresh mass (m_F) and fresh volume (V_F) via water displacement on an analytical balance. Then, they were submerged in distilled water for 24 h and weighed for saturated mass (m_S) and saturated volume (V_S).

The samples were placed in pre-weighed custom-made nickel-coated aluminum chambers with inner dimensions of 25 mm diameter and 45 mm length. The chambers were connected to Peltier-type psychrometers (Merrill Instruments, Logan, UT) and placed in a water bath at 30°C for 3 hr to equilibrate the humidity within the chambers. Then, water potential was measured using an automated multi-channel micro-voltmeter (CR7, Campbell Scientific, Logan, UT) with a 10 s thermocouple cooling current. For samples with water potential <−4 MPa, a 45 s cooling current was used to improve accuracy. Each psychrometer probe was calibrated against salt solutions beforehand, and the plateau of the psychromatic response curve was used to assess water potential.

After the initial measurement of water potential, the chambers were opened and the samples were allowed to air dry for periods of 0.5–2 hr. Then, mass and water potential were re-measured. This process was repeated until water potential reached <−7 MPa. Dry mass was measured after drying the samples at 65°C for >72 hr.

At each point, cumulative water released from the sample was calculated as follows:

$$\text{Cumulative water release} = \frac{m_S - m_F}{V_S}$$

Cumulative water release was plotted against water potential to construct the water release curves. Non-linear regression was used to fit a Gompertz function through each water release curve. The point at which the curve began to asymptote was taken as the point of maximum change in slope (i.e., the point where the third derivative equaled zero, a.k.a the "elbow" of the cumulative water release curve; C_{ELBOW}; MPa) (Meinzer et al., 2009). Sapwood capacitance (C_{SW}; kg m^{-3} MPa^{-1}) was taken as the slope between this point and the origin. Raw cumulative water release curves with fitted functions are presented in Figure S3.

2.6 | Mortality rates

Species-specific instantaneous mortality rates were determined from the ForestGEO tree census data, which is publicly available through the ForestGEO Data Portal (http://ctfs.si.edu/datarequest/) (Condit, 1998; Condit et al., 2009, 2019a, 2020; Hubbell et al., 1999). ForestGEO research plots are censused every 5 years, which involves identifying, tagging, and measuring all free-standing trees with a diameter at breast height (DBH) greater than 1 cm. We calculated two mortality rates, the first using the 1995 and 2000 Barro

Colorado Islanded censuses as these captured the 1997–1998 El Niño and hence mortality trends associated with moisture stress, and the 2010 and 2015 censuses, as these were the most recently available censuses. We used the "mortality_ctfs()" function in the "fgeo" package (ver. 1.1.4) to calculate species-specific instantaneous mortality rates as follows:

$$Z = \frac{\log(N) - \log(S)}{\text{time}}$$

where N is the number of individuals alive in the first census and S is the number of survivors (i.e., all individuals alive in both censuses). We filtered our mortality calculation to include only individuals with a minimum DBH of 20 cm, as we measured traits on mature canopy trees and mortality rates can vary among size classes.

2.7 | Species-specific optimal moisture

Condit et al. (2013) determined tree species composition for 72 sites across the same rainfall gradient and modeled species' occurrence as a function of eight environmental factors, including dry-season intensity. Dry-season intensity was calculated as the cumulative moisture deficit D_{ij} between days i and j during the dry season as follows:

$$D_{ij} = \sum_{t=i}^{j} (P_t - E_t)$$

where P_t was precipitation on day t and E_t was potential evapotranspiration on day t. When E_t exceeds P_t, as occurs during the dry season, D_{ij} takes negative values. The minimum D_{ij} for a year was their measure of dry-season severity, and because the minimum D_{ij} is a negative value, the higher (or less negative) the value, the moister it is. Condit et al. (2013) found that regional distributions were strongly affected by dry-season intensity for 57.6% of the 550 species present at 10 or more of their 72 sites. Using their fitted coefficients relating probability of occurrence to D_{ij} for each of our study species, we calculated each species' optimal position across the central Panama rainfall gradient. More positive values indicate a species is associated with moister sites and more negative values indicate a species is associated with drier sites. We use this optimal position along the rainfall gradient as a proxy for species-specific optimal moisture, and the higher a species' optimal moisture, the more dependent it is on moisture.

2.8 | Statistics

Two hydraulic safety margins (HSMs) were calculated relative to minimum seasonal water potential (Ψ_{MIN}), including (1) Ψ_{MIN}–π_{TLP} and (2) Ψ_{MIN}–C_{ELBOW}. For HSMs, a more positive value indicates a safer strategy as the water status of the plant has not exceeded the threshold measure, while a more negative value indicates a riskier strategy as the water status of the plant has exceeded the threshold measure.

Prior to analyses, variables were tested for normality using the Shapiro–Wilk test with the "stats" package (ver. 3.5.2). Variables that were not normally distributed were log transformed, except Ψ_{MIN}–C_{ELBOW} because it had both positive and negative values.

We conducted an initial test for differences in measured traits (LMA, LDMC, A_L:A_{SW}, ρ_{SW}, C_{ELBOW}, C_{SW}, Ψ_{MIN}, π_{TLP}, $\Delta\Psi$, Ψ_{MIN}–π_{TLP}, Ψ_{MIN}–C_{ELBOW}, optimal moisture, and mortality rate) between leaf habit (evergreen or deciduous), but found no differences in traits between leaf habit except for ρ_{SW}. As this did not have a major impact on our results, we proceeded with testing for differences in measured traits among sites (hypothesis 1) using MANOVA with the "stats" package, as these represented multiple dependent variables for the independent variable of site, with each species serving as a replicate.

To test for coordination among species' hydraulic traits and with moisture dependency and mortality (hypothesis), we conducted an initial principal components analysis, presented in Figure S4. Then, we tested for correlations using Pearson's correlation ($\alpha = 0.05$), with each species serving as a replicate, using the "rcorr" function in the "Hmisc" package (ver. 4.2). Using the results from the correlation matrix and following Rosas et al. (2019), we characterized a hydraulic trait covariation network, with each trait treated as a node and each significant correlation treated as an edge that connected nodes (hypothesis 3). The nodes and edges were graphed with the "igraph" package (Csardi & Nepusz, 2006). Two indicators of network centrality were calculated for each trait/node: (1) the degree of network centrality (D), defined as the number of edges for a node, and (2) the weighted degree of network centrality (D_W), defined as the sum of the absolute values of all significant Pearson's correlation coefficients for each node.

All statistics were done with R (ver. 3.5.2) (R Core Team, 2020) in R Studio (ver. 1.1.463). Data associated with water potentials in this study are publicly available at the NGEE-Tropics dataset archive (Ely et al., 2019; Wolfe et al., 2019). Traits, their units, and corresponding symbol used in this manuscript are in Table 2.

3 | RESULTS

There was no significant difference among sites for Ψ_{MIN}, $\Delta\Psi$, π_{TLP}, Ψ_{MIN}–π_{TLP}, C_{ELBOW}, Ψ_{MIN}–C_{ELBOW} (Figure 2), A_L:A_{SW}, LMA, LDMC, ρ_{SW}, C_{SW}, (Figure 3), optimal moisture, or mortality (Figure 4) despite large differences in site-specific precipitation (Figure 1a).

There was coordination among traits (Figure 5), with LMA positively correlated with LDMC ($p = 0.0001$; $r = 0.68$) and negatively correlated with A_L:A_{SW} ($p = 0.03$; $r = -0.44$). ρ_{SW} was positively correlated with C_{ELBOW} ($p = 0.0500$; $r = 0.38$) and C_{SW} ($p = 0.0003$; $r = -0.64$). C_{SW} was also correlated with Ψ_{MIN} ($p = 0.01$; $r = 0.53$), $\Delta\Psi$ ($p = 0.02$; $r = 0.50$), Ψ_{MIN}–π_{TLP} ($p = 0.02$; $r = 0.49$), and Ψ_{MIN}–C_{ELBOW} ($p = 0.047$; $r = 0.42$); species with greater sapwood capacitance had less negative

TABLE 2 Measured traits with their corresponding symbol and units, along with the descriptors of the trait network across 27 study species from 3 sites in Panama with varying mean annual precipitation

Trait	Symbol	Units	*D*	D_W
Path 1				
Turgor loss point	π_{TLP}	MPa	2	0.98
Instantaneous mortality rate			2	1.14
Elbow of cumulative water release curve	C_{ELBOW}	MPa	2	1.26
Sapwood density	ρ_{SW}	g/cm^3	2	1.02
Minimum seasonal water potential	Ψ_{MIN}	MPa	4	2.7
Minimum seasonal water potential minus maximum seasonal water potential	$\Delta\Psi$	MPa	4	2.75
Sapwood capacitance	C_{SW}	$kg\ m^{-3}\ MPa^{-1}$	5	2.56
Minimum seasonal water potential minus elbow of cumulative water release curve	Ψ_{MIN}–C_{ELBOW}	MPa	5	2.81
Minimum seasonal water potential minus turgor loss point	Ψ_{MIN}–π_{TLP}	MPa	6	3.58
Path 2				
Leaf dry matter content	LDMC	g/g	1	0.68
Optimal moisture			1	0.48
Leaf mass per area	LMA	g/m^2	2	1.12
Leaf area to sapwood area ratio	A_L:A_{SW}	m^2/m^2	2	0.92

Note: The degree of network centrality (*D*) is defined as the number of edges per node. The weighted degree of network centrality (D_W) is defined as the sum of absolute values for all significant coefficients of correlation for a node.

minimum seasonal water potential, a smaller change in water potential over the dry season, a greater or more positive Ψ_{MIN}–π_{TLP} safety margin, and a greater or more positive Ψ_{MIN}–C_{ELBOW} safety margin. Ψ_{MIN} was also positively correlated with $\Delta\Psi$ ($p < 0.0001$; $r = 0.95$), Ψ_{MIN}–π_{TLP} ($p = 0.001$; $r = 0.72$), and Ψ_{MIN}–C_{ELBOW} ($p = 0.01$; $r = 0.52$); species with a more negative minimum seasonal water potential had a greater change in water potential over the dry season, a smaller or more negative Ψ_{MIN}–π_{TLP} safety margin, and a smaller or more negative Ψ_{MIN}–C_{ELBOW} safety margin. In addition, $\Delta\Psi$ was positively correlated with Ψ_{MIN}–π_{TLP} ($p = 0.0005$; $r = 0.78$) and Ψ_{MIN}–C_{ELBOW} ($p = 0.01$; $r = 0.52$); species with a greater change in water potential over the dry season also had a smaller or more negative Ψ_{MIN}–π_{TLP} safety margin and Ψ_{MIN}–C_{ELBOW} safety margin. Ψ_{MIN}–π_{TLP} was correlated with Ψ_{MIN}–C_{ELBOW} ($p = 0.02$; $r = -0.48$) and π_{TLP} ($p = 0.02$; $r = 0.48$); species with a greater or more positive Ψ_{MIN}–π_{TLP} safety margin had a greater or more positive Ψ_{MIN}–C_{ELBOW} safety margin, a more resistant or more negative turgor loss point. 2010–2015 mortality rates were correlated with π_{TLP} ($p = 0.048$; $r = -0.5$) and Ψ_{MIN}–π_{TLP} ($p = 0.02$; $r = -0.64$); species with a greater or more positive Ψ_{MIN}–π_{TLP} safety margin had a lower mortality rate. As the 1995–2000 mortality rates were also correlated with π_{TLP} ($p = 0.048$; $r = -0.51$) and Ψ_{MIN}–π_{TLP} ($p = 0.03$; $r = -0.57$), we excluded them from further analysis (Figure S5). Ψ_{MIN}–C_{ELBOW} and C_{ELBOW} were positively correlated ($p < 0.0001$; $r = 0.88$). The only trait that was correlated with species-specific optimal moisture was A_L:A_{SW} ($p = 0.01$; $r = -0.48$), with more moisture-dependent species having a lower A_L:A_{SW} and less moisture-dependent species having a higher A_L:A_{SW} (Figure 6).

An analysis of network centrality for these measured traits (Figure 5) revealed that the HSM Ψ_{MIN}–π_{TLP} was the most connected trait, with a degree of network centrality (*D*) equal to 6 (Table 2). C_{SW} and Ψ_{MIN}–C_{ELBOW} were the next most connected traits, each with *D* equal to 5. Furthermore, Ψ_{MIN}–π_{TLP} also had the highest weighted degree of network centrality (D_W), with $D_W = 3.58$ (Table 2), followed by Ψ_{MIN}–C_{ELBOW} ($D_W = 2.81$), $\Delta\Psi$ ($D_W = 2.75$), Ψ_{MIN} ($D_W = 2.7$), and C_{SW} ($D_W = 2.56$).

4 | DISCUSSION

We investigated plant hydraulic traits, including hydraulic safety margins (HSMs), during an intense drought triggered by the 2015–2016 El Niño event on 27 dominant canopy tree species at three sites with differing historical precipitation across the isthmus of Panama. We capitalized on the drought event as a time when plant water status might approach or exceed thresholds of water stress, resulting in small or negative HSMs. We investigated how plant hydraulic traits vary among a diverse set of dominant tree species across a tropical rainfall gradient and related these traits to species-specific optimal moisture and mortality rates. We found there were no differences in any measured trait among sites (Figures 2–4), opposing our first hypothesis that hydraulic traits would vary across sites with different long-term mean annual precipitation. We did find hydraulic trait coordination, with HSMs correlated with multiple other traits, supporting our second hypothesis (Figure 5). In addition, π_{TLP} and Ψ_{MIN}–π_{TLP} were the only traits correlated with mortality rate (Figure 5). Finally, we found that A_L:A_{SW} was the only trait correlated with species-specific optimal moisture, with more moisture-dependent species (i.e., those with a higher optimal moisture value) having lower A_L:A_{SW} and less moisture-dependent species having higher A_L:A_{SW} (Figure 6).

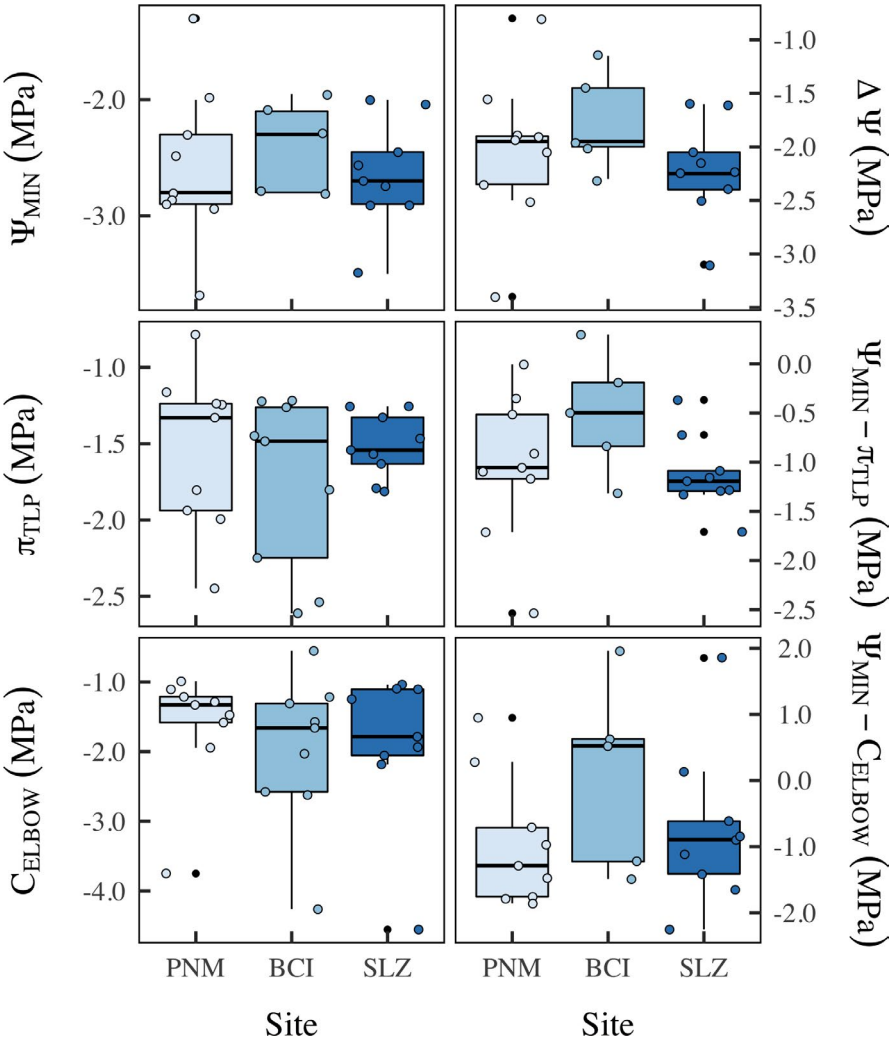

FIGURE 2 Minimum seasonal water potential (Ψ_{MIN}; MPa), the difference between the minimum seasonal water potential and maximum seasonal water potential ($\Delta\Psi$; MPa), turgor loss point (π_{TLP}; MPa), the difference between the minimum seasonal water potential and turgor loss point ($\Psi_{MIN}-\pi_{TLP}$; MPa), the "elbow" of the cumulative water release curve (C_{ELBOW}; MPa), and the difference between the minimum seasonal water potential and the "elbow" of the cumulative water release curve ($\Psi_{MIN}-C_{ELBOW}$; MPa) measured at Parque Natural Metropolitano (PNM; light blue), Barro Colorado Island (BCI; medium blue), and Fort San Lorenzo (SLZ; dark blue) in Panama during the 2015–2016 El Niño. The boxplots display the median as a bold horizontal line, with colored hinges above and below the median to illustrate the 25th and 75th percentile. Outliers, values more than 1.5 times the inter-quartile range, are displayed as individual black points. The raw data points are overlaid on the boxplots as color-filled points. There were no significant differences between sites (α = 0.05) for any trait

Acute drought can be fatal for many plant species, as plants are sessile and unable to move to escape detrimental conditions. The probability of surviving is thought to be higher for species that typically operate well within a safe range of water potentials, that is, have a larger HSM. Species that "live on the edge" and routinely experience water potentials close to levels of desiccation (i.e., have a smaller hydraulic safety margin) may be more likely to suffer drought mortality. Classically, HSMs are reported as the minimum water potential relative to xylem vulnerability to cavitation, specifically the water potential at 50% or 88% loss of conductivity (Ψ_{50} and Ψ_{88}, respectively). However, cavitation resistance is not the only threshold for water stress. Other thresholds, including the water potential at stomatal closure, the turgor loss point, or significant depletion of sapwood capacitance, can be indicators of safety from hydraulic failure. We found $\Psi_{MIN}-\pi_{TLP}$ was correlated with species-specific mortality rates (Figure 5); species with larger $\Psi_{MIN}-\pi_{TLP}$ safety margins had lower mortality rates, indicating that species whose water status exceeded their turgor loss point are more likely to die during drought. Turgor loss point is often used as a proxy for the water potential at stomatal closure, which occurs to avoid hydraulic failure in the vascular system (Bartlett et al., 2016; Martin-StPaul et al., 2017). In a seasonally dry tropical forest, Powers (2020) used a similar foliar hydraulic safety margin (the difference between the water potential at 50% of leaf embolism and the turgor loss point) rather than the "classic" stem Ψ_{50} or Ψ_{88}, and they found that species with a larger HSM were associated with lower mortality (Powers, 2020). This further supports the link between hydraulic traits and mortality (Anderegg et al., 2016), with hydraulic failure as a likely causal mechanism. We also found no differences in any HSM among sites, despite a wide sampling of canopy tree species as well as large historical differences in precipitation between sites. Previous studies have found similar trends. For example, two tropical forests with contrasting precipitation in the Amazon had similar hydraulic safety margins ($\Psi_{MIN}-\Psi_{50}$ and $\Psi_{MIN}-\Psi_{88}$) during the same 2015–2016 El Niño as our present study (Barros et al., 2019). In addition, at the same sites as our present study, while there were large differences in non-structural carbohydrates (NSC) among species, there were no seasonal differences in NSC as the drought progressed nor were there differences among sites (Dickman et al., 2019). Furthermore, an additional study found no differences in sap flux or sap flux sensitivity to VPD among these sites (Grossiord, 2019). One explanation could be that despite large variation in mean annual precipitation among sites, water is not a limiting factor for this system. It is also possible that water is in fact limiting, and the degree of limitation is

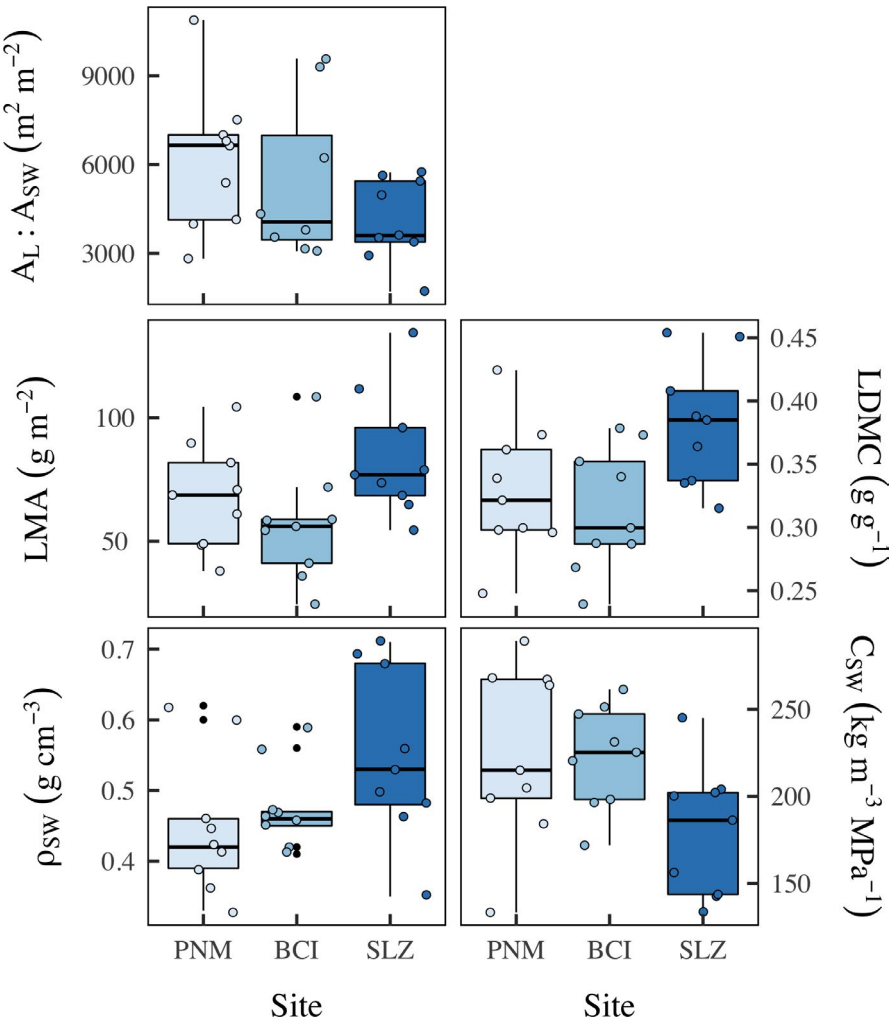

FIGURE 3 Leaf area to sapwood area ratio (A_L:A_{SW}; m^2/m^2), leaf mass per area (LMA; g/m^2), leaf dry matter content (LDMC; g/g), sapwood density (ρ_{SW}; g/cm^3), and sapwood capacitance (C_{SW}; kg m^{-3} MPa^{-1}) measured at Parque Natural Metropolitano (PNM; light blue), Barro Colorado Island (BCI; medium blue), and Fort San Lorenzo (SLZ; dark blue) in Panama during the 2015–2016 El Niño. The boxplots display the median as a bold horizontal line, with colored hinges above and below the median to illustrate the 25th and 75th percentile. Outliers, values more than 1.5 times the inter-quartile range, are displayed as individual black points. The raw data points are overlaid on the boxplots as color-filled points. There were no significant differences between sites (α = 0.05) for any trait

the same across sites. Another explanation is that HSMs are tightly constrained (Choat et al., 2012), even when using a water stress threshold besides Ψ_{50}.

It should be noted that a number of study species had negative HSMs, meaning the water status of the plant exceeded the defined thresholds of water stress. It is likely that the exceptional drought conditions present during the time of our study drove species beyond their typical range of plant water potentials, as was also seen in Tan et al. (2020). This is supported by the evidence that multiple measures of HSM were negative (Figure 3). Furthermore, in the sequence of drought response traits, leaf wilting (π_{TLP}) occurs before 50% loss and 88% loss of stem hydraulic conductivity (Ψ_{50} and Ψ_{88}, respectively) (Bartlett et al., 2016), so negative HSMs based on Ψ_{MIN}–π_{TLP} would occur more frequently and be more common that stem vulnerability curve-based HSMs (such as Ψ_{MIN}–Ψ_{50} or Ψ_{MIN}–Ψ_{88}). Calculation of Ψ_{MIN}–Ψ_{50} using independent vulnerability curves measured using the pneumatic method (Pereira et al., 2016) for a subset of our species independently corroborate negative HSMs (Medina *unpublished data*; Smith-Martin *unpublished data*), though the pneumatic method is potentially subject to artifacts with long-vessel species (Sergent et al., 2020).

Our trait network analysis highlights the diversity of drought adaptation strategies present among moist tropical forest trees, with mechanistic implications for drought responses (Figure 5). Network analysis is often applied to social networks to identify the most influential person, or in epidemiology to identify disease super-spreaders. However, Rosas et al. (2019) recently applied network analysis to examine plant hydraulic trait relationships with water availability within species (Rosas et al., 2019). Here, we examined trait relationships among species and included HSMs. We found that traits grouped into two network paths. In the largest path, we confirm classic trade-offs, such as between sapwood density and capacitance (McCulloh et al., 2014; Pratt & Jacobsen, 2017; Pratt et al., 2007; Santiago et al., 2018; Savi et al., 2017; Scholz et al., 2007; Trifilò et al., 2015). In fact, we found that sapwood capacity and HSMs (Ψ_{MIN}–π_{TLP} and Ψ_{MIN}–C_{ELBOW}) were among the most connected traits, having the highest degree of network centrality and among the top weighted degree of network centrality, which is explained by the integrative nature of these traits (Table 2). In addition, π_{TLP} and Ψ_{MIN}–π_{TLP} were the only traits correlated with mortality rate. In the second path, we found that leaf functional traits grouped together, including

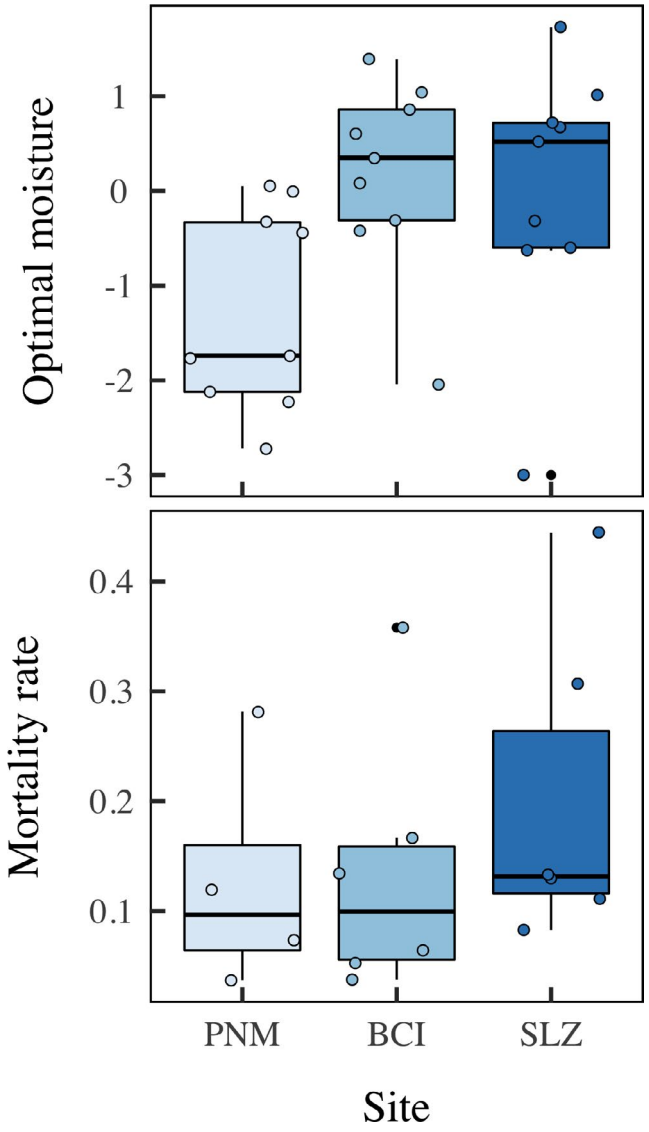

FIGURE 4 Optimal moisture and instantaneous mortality rate for species measured at Parque Natural Metropolitano (PNM; light blue), Barro Colorado Island (BCI; medium blue), and Fort San Lorenzo (SLZ; dark blue) in Panama during the 2015–2016 El Niño. Mortality rates were calculated from the 2010 and 2015 BCI censuses and filtered to include trees with a minimum diameter at breast height (DBH) of 20 cm. The boxplots display the median as a bold horizontal line, with colored hinges above and below the median to illustrate the 25th and 75th percentile. Outliers, values more than 1.5 times the inter-quartile range, are displayed as individual black points. The raw data points are overlaid on the boxplots as color-filled points. There were no significant differences between sites (α = 0.05) for any trait

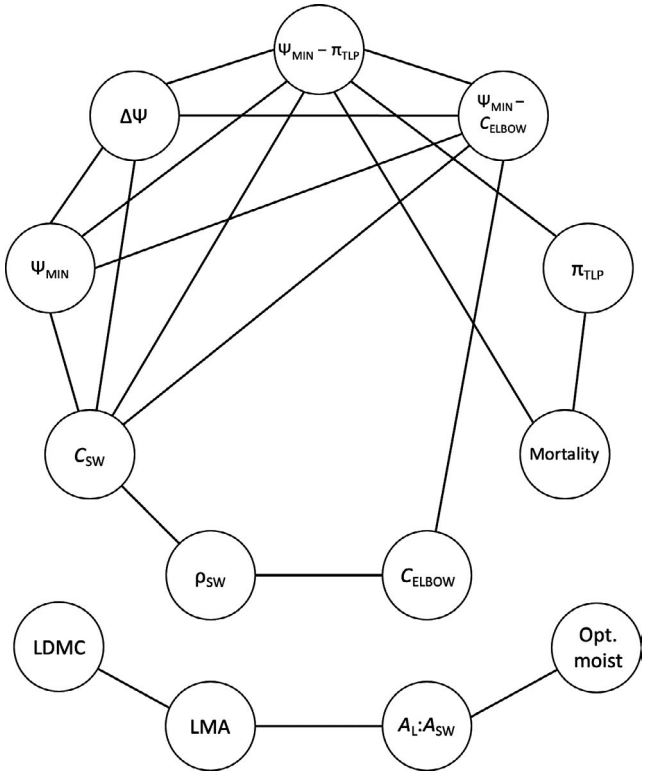

FIGURE 5 Trait network analysis for species measured at Parque Natural Metropolitano, Barro Colorado Island, and Fort San Lorenzo in Panama during the 2015–2016 El Niño. Each trait represents a node in the network, and each significant correlation represents an edge in the network. Corresponding trait names for each node, along with the degree and weighted degree of network centrality, are in Table 2

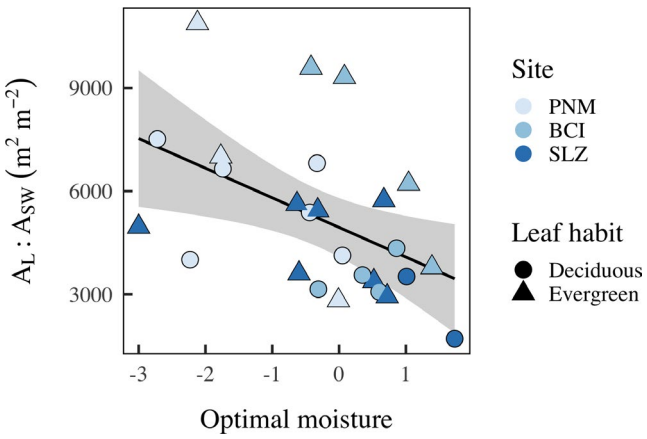

FIGURE 6 Correlation between species-specific optimal moisture and leaf area to sapwood area ratio (A_L:A_{SW}; m/m^2) measured at Parque Natural Metropolitano (PNM; light blue), Barro Colorado Island (BCI; medium blue), and Fort San Lorenzo (SLZ; dark blue) in Panama during the 2015–2016 El Niño. Leaf habit (i.e., deciduousness) is indicated by the symbol shape. Higher optimal moisture values mean a species is more highly associated with wet sites and therefore more moisture-dependent

LDMC, LMA, and A_L:A_{SW}. Furthermore, species-specific optimal moisture was a node in this path, and the only trait in our study that it was correlated with was A_L:A_{SW}; more moisture-dependent species (i.e., higher optimal moisture value) had lower A_L:A_{SW}, and less moisture-dependent species (i.e., lower optimal moisture value) had higher A_L:A_{SW}. While some within-path relationships

are explained by a commonality, such as Ψ_{MIN}, $\Delta\Psi$, and HSMs, and also leaf dry mass in LDMC and LMA, this does not negate the meaningful mechanisms underlying these relationships nor does it take away from the independence of the two network paths.

A_L:A_{SW}, the inverse of which is called the Huber value (Tyree & Ewers, 1991), represents the total transpiring leaf area that must be supplied with water by the sapwood area and is associated with pipe model theory (Shinozaki et al., 1964). Previous research has shown that hydraulic architecture plays a major role in regulating plant water use (Trugman, Anderegg, Sperry, et al., 2019; Trugman, Anderegg, Wolfe, et al., 2019) and is therefore a determinant of woody plant drought tolerance (Pivovaroff et al., 2016). Here, however, the relationship is at first surprising given that more moisture-dependent species in fact have a lower A_L:A_{SW}. One might assume that species associated with wetter sites would have the moisture availability to support a larger transpiring leaf area. Here, however, leaf phenology is a key aspect to the relationship. While our *a priori* species selection criteria required study species to have leaves at the time of our field campaign during the dry season, this did not mean that all study species were in fact evergreen (Table 1). Deciduousness runs along a continuum, and we included a number of species that were obligate deciduous, facultative deciduous, and brevideciduous (leaf shed is followed by immediate flushing (Eamus & Prior, 2001)). For these deciduous species, our field campaigns did not happen to align with the timing of their leaf shedding. We find that more species have a deciduous leaf phenology at the driest site (eight out of nine study species are deciduous at PNM) versus the wettest site (three out of nine study species are deciduous at SLZ). These deciduous species only have to support a large leaf area for part of the year and can drop their leaves when conditions are less favorable, that is, low moisture availability. Conversely, species found at moister sites having a lower A_L:A_{SW}, but they maintain this leaf area year-round. This is why five of the six species with an optimal moisture less than −1 are deciduous (Figure 6). This is further supported by evidence from seasonally dry tropical forests, which the follow the general relationship of evergreen species having smaller A_L:A_{SW} (or higher Huber values) and deciduous species have larger A_L:A_{SW} (or smaller Huber values) (Eamus & Prior, 2001).

Understanding the physiological mechanisms that underlie tropical tree responses to intensified droughts helps us understand tree survival and mortality, which have implications for tropical forest dynamics and biogeochemical cycles (Cavaleri et al., 2017). Our finding that hydraulic architecture was the only trait that explained species' moisture dependency reveals that while HSMs are important traits for understandings species' drought tolerance and mortality risk (Anderegg et al., 2016), other traits warrant attention as well.

ACKNOWLEDGEMENTS

This work was supported by the Next-Generation Ecosystem Experiments (NGEE Tropics) projects that was supported by the Office of Biological and Environmental Research in the Department of Energy, Office of Science. AR and SPS were supported by the United States Department of Energy contract No. DE-SC0012704 to Brookhaven National Laboratory. CG was supported by the Swiss National Science Foundation SNF (PZ00P3_174068). BTW was supported by the National Institute of Food and Agriculture, U.S. Department of Agriculture, McIntire Stennis project under LAB94493. The BCI forest dynamics research project was made possible by National Science Foundation (NSF) grants to Stephen P. Hubbell, with support from the Forest Global Earth Observatory, the Smithsonian Tropical Research Institute, the John D. and Catherine T. MacArthur Foundation, the Mellon Foundation, the Small World Institute Fund, and numerous private individuals, and through the hard work of over 100 people from 10 countries over the past three decades. The plot project is part the Forest Global Earth Observatory (ForestGEO), a global network of large-scale demographic tree plots. The CTFS R Package was developed with the support of NSF grant #1046113 to Stuart J. Davies through the NSF-IRCN program on the Dimensions of Biodiversity. Special thanks to Laura Fernandez De Una for translating our abstract to Spanish.

CONFLICT OF INTEREST

No potential conflict of interest was reported by the authors.

AUTHOR CONTRIBUTION

Alexandria L. Pivovaroff involved in conceptualization, formal analysis, methodology, visualization, writing—original draft, and writing—review and editing. **Nate McDowell** involved in conceptualization, supervision, and writing—review and editing. **Brett T. Wolfe** involved in investigation, formal analysis, data curation, resources, and writing—review and editing. **Bradley Christoffersen, L. Turin Dickman, Charlotte Grossiord, Shawn P. Serbin, Jin Wu, and Chonggang Xu** involved in writing—review and editing. **Stuart Davies** involved in data curation and writing—review and editing. **Riley T. Leff** involved in software and writing—review and editing. **Alistair Rogers** involved in resources and writing—review and editing. **S. Joseph Wright** involved in methodology, resources, and writing—review and editing. **Jeffrey Q. Chambers** involved in funding acquisition and supervision.

DATA AVAILABILITY STATEMENT

Meteorological data for these sites are publicly available from the Smithsonian Tropical Research Institute "Physical Monitoring Program" site (http://biogeodb.stri.si.edu/physical_monitoring/research/). ForestGEO census data for tree species at these sites, which were used to calculate species-specific mortality rates, are publicly available through the ForestGEO Data Portal (http://ctfs.si.edu/datarequest/). Data related to the fitted coefficients relating probability of occurrence to dry-season intensity for each of our study species, which were used to calculate species-specific optimal moisture, are available in the supplemental data for Condit et al., 2013. Data related to water potentials in this study are available at the NGEE-Tropics dataset archive (Ely et al., 2019; Wolfe et al., 2019). The raw pressure–volume curves and stem water release curves are presented in the Supplemental Information (Figures S1 and S3, respectively). In addition, a summary of the trait means is presented in Table S1.

ORCID

Alexandria L. Pivovaroff https://orcid.org/0000-0002-3104-1900

S. Joseph Wright https://orcid.org/0000-0003-4260-5676

REFERENCES

Allen, C. D., Breshears, D. D., & McDowell, N. G. (2015). ESA CENTENNIAL PAPER On underestimation of global vulnerability to tree mortality and forest die-off from hotter drought in the Anthropocene. *Ecosphere*, *6*, 1–55.

Anderegg, W. R. L. (2015). Spatial and temporal variation in plant hydraulic traits and their relevance for climate change impacts on vegetation. *New Phytologist*, *205*, 1008–1014.

Anderegg, W. R. L., Klein, T., Bartlett, M., Sack, L., Pellegrini, A. F. A., Choat, B., & Jansen, S. (2016). Meta-analysis reveals that hydraulic traits explain cross-species patterns of drought-induced tree mortality across the globe. *Proceedings of the National Academy of Sciences*, *113*, 2–7.

Baillie, I. C., Ashton, P. S., Court, M. N., Fitzpatrick, E. A., Tinsley, J., & Anderson, J. A. R. (1987). Site characteristics and the distribution of tree species in mixed dipterocarp forest on tertiary sediments in central sarawak, malaysia. *Journal of Tropical Ecology*, *3*, 201–220.

Barros, F. D. V., Bittencourt, P. R. L., Brum, M., Restrepo-Coupe, N., Pereira, L., Teodoro, G. S., Saleska, S. R., Borma, L. S., Christoffersen, B. O., Penha, D., Alves, L. F., Lima, A. J. N., Carneiro, V. M. C., Gentine, P., Lee, J.-E., Aragão, L. E. O. C., Ivanov, V., Leal, L. S. M., Araujo, A. C., & Oliveira, R. S. (2019). Hydraulic traits explain differential responses of Amazonian forests to the 2015 El Niño-induced drought. *New Phytologist*, *223*, 1253–1266.

Bartlett, M. K., Klein, T., Jansen, S., Choat, B., & Sack, L. (2016). The correlations and sequence of plant stomatal, hydraulic, and wilting responses to drought. *Proceedings of the National Academy of Sciences of the United States of America*, *113*, 13098–13103.

Bhaskar, R., & Ackerly, D. D. (2006). Ecological relevance of minimum seasonal water potentials. *Physiologia Plantarum*, *127*, 353–359.

Blackman, C. J., Pfautsch, S., Choat, B., Delzon, S., Gleason, S. M., & Duursma, R. A. (2016). Toward an index of desiccation time to tree mortality under drought. *Plant, Cell and Environment*, *39*, 2342–2345.

Bongers, F., Poorter, L., Rompaey, R. S. A. R., & Parren, M. P. E. (1999). Distribution of twelve moist forest canopy tree species in Liberia and Côte d'Ivoire: response curves to a climatic gradient. *Journal of Vegetation Science*, *10*, 371–382.

Brienen, R. J. W., Phillips, O. L., Feldpausch, T. R., Gloor, E., Baker, T. R., Lloyd, J., Lopez-Gonzalez, G., Monteagudo-Mendoza, A., Malhi, Y., Lewis, S. L., Vásquez Martinez, R., Alexiades, M., Álvarez Dávila, E., Alvarez-Loayza, P., Andrade, A., Aragão, L. E. O. C., Araujo-Murakami, A., Arets, E. J. M. M., Arroyo, L., … Zagt, R. J. (2015). Long-term decline of the Amazon carbon sink. *Nature*, *519*(7543), 344–348. https://doi.org/10.1038/nature14283

Brodribb, T. J., & Cochard, H. (2009). Hydraulic Failure Defines the Recovery and Point of Death in Water-Stressed Conifers. *Plant Physiology*, *149*, 575–584.

Cavaleri, M. A., Coble, A. P., Ryan, M. G., Bauerle, W. L., Loescher, H. W., & Oberbauer, S. F. (2017). Tropical rainforest carbon sink declines during El Niño as a result of reduced photosynthesis and increased respiration rates. *New Phytologist*, *216*, 136–149.

Choat, B., Jansen, S., Brodribb, T. J., Cochard, H., Delzon, S., Bhaskar, R., Bucci, S. J., Feild, T. S., Gleason, S. M., Hacke, U. G., Jacobsen, A. L., Lens, F., Maherali, H., Martínez-Vilalta, J., Mayr, S., Mencuccini, M., Mitchell, P. J., Nardini, A., Pittermann, J., … Zanne, A. E. (2012). Global convergence in the vulnerability of forests to drought. *Nature*, *491*(7426), 752–755. https://doi.org/10.1038/nature11688

Condit, R. (1998). *Tropical forest census plots*. Springer Verlag.

Condit, R., Engelbrecht, B. M. J., Pino, D., Perez, R., & Turner, B. L. (2013). Species distributions in response to individual soil nutrients and seasonal drought across a community of tropical trees. *Proceedings of the National Academy of Sciences*, *110*, 5064–5068.

Condit, R., Hubbell, S. P., & Foster, R. B. (1995). Mortality Rates of 205 Neotropical Tree and Shrub Species and the Impact of a Severe. *Ecological Monographs*, *65*, 419–439.

Condit, R., Perez, R., Aguilar, S., & Lao, S. (2009). *Sherman 6-ha Forest Census Plot Data*. https://forestgeo.si.edu/sites/neotropics/sherman/sherman-plot-data

Condit, R., Perez, R., Aguilar, S., Lao, S., Foster, R., & Hubbell, S. (2019a). Complete data from the Barro Colorado 50-ha plot: 423617 trees, 35 years, v3. *DataONE*, Dataset. https://doi.org/10.15146/5xcp-0d46

Condit, R., Perez, R., Aguilar, S., Lao, S., Foster, R., & Hubbell, S. P. (2020). BCI 50-ha plot taxonomy. *Dryad (Dataset)*. https://doi.org/10.15146/R3FH61

Condit, R., Pérez, R., Lao, S., Aguilar, S., & Hubbell, S. P. (2017). Demographic trends and climate over 35 years in the Barro Colorado 50 ha plot. *Forest Ecosystems*, *4*, 1–13.

Csardi, G., & Nepusz, T. (2006). The igraph software package for complex network research. *InterJournal Complex System*, Complex Systems, 1695. https://cran.r-project.org/web/packages/igraph/citation.html

Dickman, L. T., McDowell, N. G., Grossiord, C., Collins, A. D., Wolfe, B. T., Detto, M., Wright, S. J., Medina-Vega, J. A., Goodsman, D., Rogers, A., Serbin, S. P., Wu, J., Ely, K. S., Michaletz, S. T., Xu, C., Kueppers, L., & Chambers, J. Q. (2019). Homoeostatic maintenance of nonstructural carbohydrates during the 2015–2016 El Niño drought across a tropical forest precipitation gradient. *Plant, Cell and Environment*, *42*, 1705–1714.

Eamus, D., & Prior, L. (2001). *Ecophysiology of trees of seasonally dry tropics: Comparisons among phenologies*. Advances in Ecological Research, *32*, Academic Press.

Ely, K., Rogers, A., Serbin, S., Wu, J., Wolfe, B., Dickman, T., Collins, A., Detto, M., Grossiord, C., & McDowell, N. (2019). *Leaf sample detail, Feb2016-May2016, PA-SLZ, PA-PNM, PA-BCI: Panama*. 1.0. NGEE Tropics Data Collection.

Engelbrecht, B. M. J., Comita, L. S., Condit, R., Kursar, T. A., Tyree, M. T., Turner, B. L., & Hubbell, S. P. (2007). Drought sensitivity shapes species distribution patterns in tropical forests. *Nature*, *447*, 80–82.

Gentry, A. H. (1988). Changes in Plant Community Diversity and Floristic Composition on Environmental and Geographical Gradients. *Annals of the Missouri Botanical Garden*, *75*, 1–34.

Grossiord, C., Christoffersen, B., Alonso-Rodríguez, A. M., Anderson-Teixeira, K., Asbjornsen, H., Aparecido, L. M. T., Carter Berry, Z., Baraloto, C., Bonal, D., Borrego, I., Burban, B., Chambers, J. Q., Christianson, D. S., Detto, M., Faybishenko, B., Fontes, C. G., Fortunel, C., Gimenez, B. O., Jardine, K. J., … McDowell, N. G. (2019). Precipitation mediates sap flux sensitivity to evaporative demand in the neotropics. *Oecologia*, *191*, 519–530.

Hartmann, H., Adams, H. D., Anderegg, W. R. L., Jansen, S., Zeppel, M. J. B., & Mortality, T. (2015). Research frontiers in drought- induced tree mortality : crossing scales and disciplines. *New Phytologist*, *205*, 965–969.

Hubbell, S. P., Foster, R. B., O'Brien, S. T., Harms, K. E., Condit, R., Wechsler, B., Wright, S. J., & Loo De Lao, S. (1999). Light-gap disturbances, recruitment limitation, and tree diversity in a neotropical forest. *Science*, *283*, 554–557.

Kerstiens, G. (1996). Cuticular water permeability and its physiological significance. *Journal of Experimental Botany*, *47*, 1813–1832.

Kerstiens, G. (2006). Water transport in plant cuticles: An update. *Journal of Experimental Botany*, *57*, 2493–2499.

Koide, R. T., Robichaux, R. H., Morse, S. R., & Smith, C. M. (1991). Plant water status, hydraulic resistance and capacitance. In R. W. Pearcy, J. R. Ehleringer, H. Mooney, & P. W. Rundel (Eds.), *Plant physiological ecology: Field methods and instrumentation* (pp. 161–183). Chapman and Hall.

Martin-StPaul, N., Delzon, S., & Cochard, H. (2017). Plant resistance to drought depends on timely stomatal closure. *Ecology Letters*, *20*, 1437–1447.

McCulloh, K. A., Johnson, D. M., Meinzer, F. C., & Woodruff, D. R. (2014). The dynamic pipeline: hydraulic capacitance and xylem hydraulic safety in four tall conifer species. *Plant, Cell and Environment*, *37*, 1171–1183.

McDowell, N., Allen, C. D., Anderson-Teixeira, K., Brando, P., Brienen, R., Chambers, J., Christoffersen, B., Davies, S., Doughty, C., Duque, A., Espirito-Santo, F., Fisher, R., Fontes, C. G., Galbraith, D., Goodsman, D., Grossiord, C., Hartmann, H., Holm, J., Johnson, D. J., … Xu, X. (2018). Drivers and mechanisms of tree mortality in moist tropical forests. *New Phytologist*, *219*, 851–869.

Meinzer, F. C., James, S. A., Goldstein, G., & Woodruff, D. R. (2003). Whole-tree water transport scales with sapwood capacitance in tropical forest canopy trees. *Plant, Cell and Environment*, *26*, 1147–1155.

Meinzer, F. C., Johnson, D. M., Lachenbruch, B., McCulloh, K. A., & Woodruff, D. R. (2009). Xylem hydraulic safety margins in woody plants: coordination of stomatal control of xylem tension with hydraulic capacitance. *Functional Ecology*, *23*, 922–930.

Meinzer, F. C., & McCulloh, K. A. (2013). Xylem recovery from drought-induced embolism: where is the hydraulic point of no return? *Tree Physiology*, *33*, 331–334.

Nardini, A., Battistuzzo, M., & Savi, T. (2013). Shoot desiccation and hydraulic failure in temperate woody angiosperms during an extreme summer drought. *New Phytologist*, *200*, 322–329.

Nardini, A., Gortan, E., Ramani, M., & Salleo, S. (2008). Heterogeneity of gas exchange rates over the leaf surface in tobacco: An effect of hydraulic architecture? *Plant, Cell and Environment*, *31*, 804–812.

Osazuwa-Peters, O., Zanne, A. E., & Contributors, P. (2011). *Wood density*. Available at http://prometheuswiki.publish.csiro.au/tiki-index.php?page=Wood+density+protocol

Pereira, L., Oliveira, R. S., Bittencourt, P. R. L., Junior, M. B. M., & Barros, F. V. (2016). Plant pneumatics: stem air flow is related to embolism – new perspectives on methods in plant hydraulics Methods. *New Phytologist*, *211*(1), 357–370. https://doi.org/10.1111/nph.13905

Pivovaroff, A. L., Cook, V. M. W., & Santiago, L. S. (2018). Stomatal behavior and stem xylem traits are coordinated for woody plant species under exceptional drought conditions. *Plant, Cell and Environment*, *41*, 2617–2626.

Pivovaroff, A. L., Pasquini, S. C., De Guzman, M. E., Alstad, K. P., Stemke, J. S., & Santiago, L. S. (2016). Multiple strategies for drought survival among woody plant species. *Functional Ecology*, *30*, 517–526.

Powers, J. S., Vargas G., G., Brodribb, T. J., Schwartz, N. B., Pérez-Aviles, D., Smith-Martin, C. M., Becknell, J. M., Aureli, F., Blanco, R., Calderón-Morales, E., Calvo-Alvarado, J. C., Calvo-Obando, A. J., Chavarría, M. M., Carvajal-Vanegas, D., Jiménez-Rodríguez, C. D., Murillo Chacon, E., Schaffner, C. M., Werden, L. K., Xu, X., & Medvigy, D. (2020). A catastrophic tropical drought kills hydraulically vulnerable tree species. *Global Change Biology*, *26*, 3122–3133.

Pratt, R. B., & Jacobsen, A. L. (2017). Conflicting demands on angiosperm xylem: Tradeoffs among storage, transport and biomechanics. *Plant, Cell and Environment*, *40*, 897–913.

Pratt, R. B., Jacobsen, A. L., Ewers, F. W., & Davis, S. D. (2007). Relationships among xylem transport, biomechanics and storage in stems and roots of nine Rhamnaceae species of the California chaparral. *New Phytologist*, *174*, 787–798.

R Core Team (2020). *R: A language and environment for statistical computing*. Available at https://www.r-project.org/

Rosas, T., Mencuccini, M., Barba, J., Cochard, H., Saura-Mas, S., & Martínez-Vilalta, J. (2019). Adjustments and coordination of hydraulic, leaf and stem traits along a water availability gradient. *New Phytologist*, *223*, 632–646.

Santiago, L. S., De Guzman, M. E., Baraloto, C., Vogenberg, J. E., Brodie, M., Hérault, B., Fortunel, C., & Bonal, D. (2018). Coordination and trade-offs among hydraulic safety, efficiency and drought avoidance traits in Amazonian rainforest canopy tree species. *New Phytologist*, *218*, 1015–1024.

Savi, T., Love, V. L., Dal Borgo, A., Martellos, S., & Nardini, A. (2017). Morpho-anatomical and physiological traits in saplings of drought-tolerant Mediterranean woody species. *Trees*, *31*, 1137–1148.

Scholz, F. G., Bucci, S. J., Goldstein, G., Meinzer, F. C., Franco, A. C., & Miralles-Wilhelm, F. (2007). Biophysical properties and functional significance of stem water storage tissues in Neotropical savanna trees. *Plant, Cell and Environment*, *30*, 236–248.

Sergent, A. S., Varela, S. A., Barigah, T. S., Badel, E., Cochard, H., Dalla-Salda, G., Delzon, S., Fernández, M. E., Guillemot, J., Gyenge, J., Lamarque, L. J., Martinez-Meier, A., Rozenberg, P., Torres-Ruiz, J. M., & Martin-StPaul, N. K. (2020). A comparison of five methods to assess embolism resistance in trees. *Forest Ecology and Management*, *468*, 118175.

Shinozaki, K., Yoda, K., Hozumi, K., & Kira, T. (1964). A quantitative analysis of plant form - The pipe model theory. *Japanese Journal of Ecology*, *14*, 133–139.

Sperry, J. S., & Love, D. M. (2015). What plant hydraulics can tell us about responses to climate-change droughts. *New Phytologist*, *207*(1), 14–27. https://doi.org/10.1111/nph.13354

Tan, F., Song, H., Fu, P., Chen, Y., Siddiq, Z., & Cao, K. (2020). Hydraulic safety margins of co-occurring woody plants in a tropical karst forest experiencing frequent extreme droughts. *Agricultural and Forest Meteorology*, *292-293*, 292–293. https://doi.org/10.1016/j.agrformet.2020.108107

Trenberth, K. E., Dai, A., Van Der Schrier, G., Jones, P. D., Barichivich, J., Briffa, K. R., & Sheffield, J. (2014). Global warming and changes in drought. *Nature Climate Change*, *4*, 17–22.

Trifilò, P., Nardini, A., Gullo, M. A. L., Barbera, P. M., Savi, T., & Raimondo, F. (2015). Diurnal changes in embolism rate in nine dry forest trees: Relationships with species-specific xylem vulnerability, hydraulic strategy and wood traits. *Tree Physiology*, *35*, 694–705.

Trugman, A. T., Anderegg, L. D. L., Sperry, J. S., Wang, Y., Venturas, M., & Anderegg, W. R. L. (2019). Leveraging plant hydraulics to yield predictive and dynamic plant leaf allocation in vegetation models with climate change. *Global Change Biology*, *25*, 4008–4021.

Trugman, A. T., Anderegg, L. D. L., Wolfe, B. T., Birami, B., Ruehr, N. K., Detto, M., Bartlett, M. K., & Anderegg, W. R. L. (2019). Climate and plant trait strategies determine tree carbon allocation to leaves and mediate future forest productivity. *Global Change Biology*, *25*, 3395–3405.

Tyree, M. T., & Ewers, F. W. (1991). The hydraulic architecture of trees and other woody plants. *New Phytologist*, *119*(3), 345–360. https://doi.org/10.1111/j.1469-8137.1991.tb00035.x

Williamson, G. B., & Wiemann, M. C. (2010). Measuring wood specific gravity… correctly. *American Journal of Botany*, *97*, 519–524.

Wolfe, B. T., & Goldstein, G. (2017). Retention of stored water enables tropical tree saplings to survive extreme drought conditions. *Tree Physiology*, *37*, 469–480.

Wolfe, B., Wu, J., Ely, K., Erbin, S., Rogers, A., Dickman, T., Collins, A., Detto, M., Grossiord, C., McDowell, N., & Michaletz, S. (2019). *Leaf water potential, Feb2016-May2016, PA-SLZ, PA-PNM, PA-BCI: Panama*. 1.0. NGEE Tropics Data Collection.

SUPPORTING INFORMATION

Additional supporting information may be found online in the Supporting Information section.

How to cite this article: Pivovaroff AL, Wolfe BT, McDowell N, et al. Hydraulic architecture explains species moisture dependency but not mortality rates across a tropical rainfall gradient. *Biotropica*. 2021;53:1213–1225. https://doi.org/10.1111/btp.12964